ADVANCED ENERGY MATERIALS
www.advenergymat.de

# Interfacing Iodine-Doped Hydrothermally Carbonized Carbon with *Escherichia coli* through an "Add-on" Mode for Enhanced Light-Driven Hydrogen Production

*Kemeng Xiao, Tsz Ho Tsang, Dong Sun, Jun Liang, Hui Zhao, Zhifeng Jiang,* Bo Wang,* Jimmy C. Yu, and Po Keung Wong**

**The recently emerged photosynthetic biohybrid systems (PBSs) integrate the advantages of the light-harvesting ability of semiconductors and the catalytic power of biological metabolism. Herein, negatively charged iodine-doped hydrothermally carbonized carbon (I-HTCC) is interfaced with surface modified *Escherichia coli* cells through a facile "add-on" mode via electrostatic interactions. As a result of the photoexcited electrons, the self-assembled I-HTCC@*E. coli* biohybrid shows enhanced hydrogen production efficiency with a quantum efficiency of 9.11% under irradiation. The transduction of photoelectrons from I-HTCC to cells is the rate-limiting step for $H_2$ production and is delivered through both direct injection and the NADH/$NAD^+$-mediated pathways. The injected photoelectrons fine-tune the $H_2$ production through the formate and NADH pathways in a subtle manner. The excellent biocompatibility and photostability of the I-HTCC@*E. coli* biohybrid demonstrate its potential real-world application under sunlight. In addition, the proposed "add-on" mode is extended to a series of negatively charged common carbon-based materials with different levels of promotion effects compared with that of pure bacterial cultures. This facile and effective mode provides an insight into the rational design of the whole-cell PBSs with various semiconductors for $H_2$ production.**

## 1. Introduction

Addressing the increasingly serious energy and environmental crisis poses a challenge to improve the utilization of renewable energy like solar power. In nature, sunlight can be utilized through the photosynthesis, a biological process that has been evolved as a survival strategy rather than to solar-to-biomass (S2B) conversion.[1] It is saturated at 20% of solar intensity and operated at low conversion efficiency, with a typical value of 0.1% for most of the plants.[2] On the artificial photosynthesis end, attempts to directly harvest sunlight through solid-state semiconductors with broad light absorption are of great interest, which exceeded the light-harvesting efficiency in terms of the light reaction in natural photosynthesis.[3] Unlike the dark reactions that involves multiple highly-specific enzymatic processes,[4] the performances of synthetic catalysts suffer from poor substrate specificity, low product diversity, and high operational costs without self-repairing

K. Xiao, T. H. Tsang, D. Sun, Dr. H. Zhao, Dr. P. K. Wong
School of Life Sciences
The Chinese University of Hong Kong
Shatin, New Territories, Hong Kong SAR 999077, China
E-mail: pkwong@cuhk.edu.hk
Dr. J. Liang, Dr. B. Wang
CAS Key Laboratory of Quantitative Engineering Biology
Shenzhen Institute of Synthetic Biology
Shenzhen Institutes of Advanced Technology
Chinese Academy of Sciences
Shenzhen 518055, China
E-mail: bo.wang@siat.ac.cn
Dr. H. Zhao
Jiangsu Key Laboratory of Anaerobic Biotechnology
School of Environment and Civil Engineering
Jiangnan University
1800 Lihu Avenue, Wuxi 214122, China
The ORCID identification number(s) for the author(s) of this article can be found under https://doi.org/10.1002/aenm.202100291.
Dr. Z. Jiang
Institute for Energy Research
School of Chemistry and Chemical Engineering
Jiangsu University
Zhenjiang 212013, China
E-mail: ntjiangzf@sina.com
Dr. J. C. Yu
Department of Chemistry
The Chinese University of Hong Kong
Shatin, New Territories, Hong Kong SAR 999077, China
Dr. P. K. Wong
Institute of Environmental Health and Pollution Control
School of Environmental Science and Engineering
Guangdong University of Technology
Guangzhou 510006, China

**DOI: 10.1002/aenm.202100291**

 

ability.[5] Therefore, several photosynthetic biohybrid systems (PBSs), which combine the excellent light-capturing capacity of semiconductors and efficient catalytic fashion of biological systems, have been developed and attract great attention.[2a]

Generally, the PBSs include enzyme-based (cell-free) and whole-cell-based forms.[2a] The cell-free PBSs require extensive purification requirement of enzymes and suffer from poor enzymatic stability. The whole-cell PBSs are thus favored not only for their ability to self-replicate and self-repair, but also for the product diversity that benefits from the sophisticated metabolic pathways.[6] Among the prototypes of whole-cell PBSs, several nanoparticle-cell biohybrids were designed to achieve electrons delivery between the inorganic materials and living cells. An early demonstration of this biohybrid combined the $TiO_2$ and *Clostridium butyricum* cells for hydrogen ($H_2$) production with the mediation of photoelectrons by methyl viologen (MV).[7]Although this suspended system was easy to operate, it was restricted by the sluggish kinetics of electron transfer. A breakthrough development was made by Peidong Yang' group, in which the non-photosynthetic *Moorella thermoacetica* was self-photosensitized by the biologically precipitated CdS with enhanced acetic acid production under light.[6a] Following this work, CdS was integrated with different bacteria species including *E. coli*,[8] *Methanosarcina barkeri*,[9] *Rhodopseudomonas palustris*,[10] *Thiobacillus denitrificans*,[11] and *Geobacter sulfurreducens*[12] for solar-to-chemical (S2C) conversion. In addition, the integration of $AgInS_2/In_2S_3$,[13] InP,[14] and CdS@ZnS[15] with microorganisms have also been successfully demonstrated. Despite these promising progresses, the PBSs are still in early-stage development and the electron transfer mechanisms and interfacial effects on the biotic and abiotic interface are poorly understood.[16] These biohybrids were fabricated through either the self-defense mechanism or the endocytosis of bacterial cells, both of which required relatively complicated operation process. And the defense to toxic metal ions of living cells is rather limited and leads to a decrease in chemical production caused by the damage of cell metabolism.[17] Given the cytotoxicity and photo-erosion of these metal-based semiconductors, non-toxic photosensitizers need to be explored to improve the efficiency and durability of the biohybrid systems.[18] Within this context, alternative PBS combining the biocompatibility of material and rational design of biohybrid system with efficient electrons transfer is highly desirable.

For the biological part, chemoheterotrophic *E. coli* was selected as the workhorse for the newly developed PBSs. Compared with the photosynthetic or autotrophic microorganisms, the industrial properties of *E. coli* endow the designed system with great prospect for practical chemical production.[19] Since understanding the interfacial charge transfer is one of the biggest challenges in the PBSs,[20] the well-established pathway of *E. coli* would contribute to reveal the underlying mechanisms.[21] As for the semiconductors, the carbon-based materials were considered as ideal candidates owing to their low toxicity, high stability, reusability, and the tunability of redox potential though material engineering.[22] Among these materials, iodine-doped hydrothermally carbonized carbon (I-HTCC) was applied in the hybrid system. It can be simply fabricated with a series of carbohydrate-based precursors including sucrose, starch, rice, grass, straw, and animal waste without emission of greenhouse gases with the addition of iodine.[23] It has been proved to possess wider light absorption and excellent charge transfer efficiency, as well as the good biocompatibility for biological integration.[23] These properties render the fabrication of *E. coli* and I-HTCC with low cost and good biocompatibility. To avoid complex integration processes and simultaneously guarantee the effective electron transfer for the PBS, exploring a facile combination method is also of great significance.

In previous studies, several cell-free biological catalytic systems have tried to employ the electrostatic interaction to assemble the biological catalytic systems with synthetic photocatalysts.[24] The yeast cells were also modified by changing surface potential to better interface with InP particles.[14] Inspired by these works, the electrostatic interactions were utilized to fabricate the PBSs in present study. On one hand, it overcomes the limitations of materials and cell types, which enables rational design of PBSs based on the practical requirement.[25] On the other hand, the electron transfer between biocatalyst and photosensitizers could also be potentially enhanced through the electrostatic interactions.[26] Therefore, for the first time, the most studied bacterium *E. coli* and the light absorber I-HTCC was self-assembled through the electrostatic interactions for $H_2$ production under light irradiation. With the simple "add-on" mode, the negatively charged I-HTCC semiconductors were easily coated on the positively charged surface of *E. coli* cells. The roles of electrons for enhancing $H_2$ production and its transduction ways at the biotic–abiotic interface had been investigated extensively. In addition, the regulation of photoelectrons in biological $H_2$ production pathways had been systematically studied. Several negatively charged carbon-based materials, including mesoporous carbon, acid-treated pollen, activated carbon, graphene, and g-$C_3N_4$ were assembled with *E. coli* cells to test the feasibility of the proposed "add-on" mode.

## 2. Results and Discussions

### 2.1. Characterization of the I-HTCC and Biohybrid System

The energy dispersive X-ray (EDX) analysis showed that the major components of the I-HTCC were carbon, oxygen, and iodine (Figure S1, Supporting Information). Through the multiple separation processes, the as-prepared I-HTCC was uniformly distributed within the particle size of 30–50 nm (**Figure 1**a). The particle size was reported as an important factor that influenced the electron–hole separation efficiency and the loading amount of catalyst on cell membranes.[8a,27] Thus, the uniform nanosized I-HTCC were beneficial for its photocatalytic activity and coating on bacterial surface. Besides, the X-ray diffraction (XRD) pattern (Figure 1c) indicated that it displayed an amorphous structure with the absence of obvious diffraction peaks. To investigate the optical features of the as-prepared I-HTCC, light absorption range and photocurrent responses were recorded. The UV-Vis diffuse reflectance spectroscopy (DRS) spectrum of I-HTCC demonstrated its wide light absorption spectrum ranging from the visible light (VL) to near-infrared (NIR) region (inset of Figure 1c), laying foundation for the excellent light utilization property of the

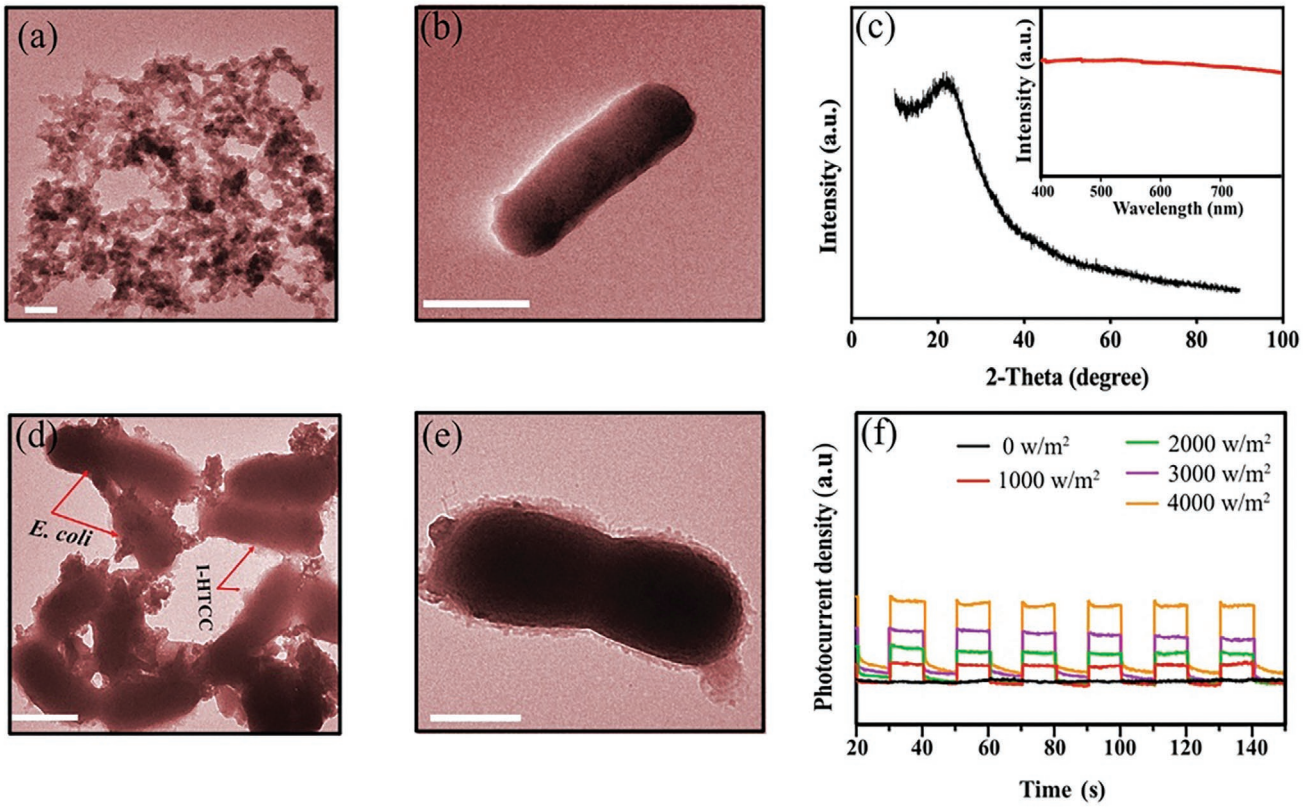


**Figure 1.** Characterization of as-prepared samples. a) TEM images of I-HTCC and b) PAH modified *E. coli* cells (scale bar: 200 nm and 1 µm). c) XRD pattern and UV–vis–DRS (inset) spectrum of I-HTCC. d,e) TEM images of I-HTCC@*E. coli* biohybrid system (scale bar: 500 nm and 1 µm). f) Photocurrent responses of I-HTCC under different light intensities.

biohybrid system. As presented in Figure 1f, the photocurrent responses of I-HTCC were prompt and reproducible under different intensities of VL, increasing with the increment of light intensity. This suggested that I-HTCC possessed good photogenerated electrons transfer efficiency. The bandgap of I-HTCC was estimated to be 1.19 eV according to the Kubelka–Munk transfer mode (Figure S2a, Supporting Information). The Mott–Schottky plot showed that I-HTCC displayed as an n-type semiconductor (Figure S2b, Supporting Information), indicating that the Fermi level ($E_f$) could be calculated from the flat potential, which was estimated to be –0.17 V. The valence band spectrum of I-HTCC suggested that the valence band maximum (VBM) to $E_f$ was 0.83 eV for I-HTCC (Figure S2c, Supporting Information). Taken together, the VBM value of I-HTCC was calculated to be 0.66 V and the conduction band minimum (CBM) was calculated to be –0.53V, accordingly (Figure S2d, Supporting Information). The excellent light absorption ability and bandgap structure of I-HTCC were benefited for transferring high-energy electrons for $H_2$ production under VL.

Initially, both the native I-HTCC and *E. coli* cells were negatively charged (Figure S3, Supporting Information), with the zeta potentials ($\zeta$) of –39.10 and –31.80 mV, respectively. The negative surface charge of living cells is due to the high density of exposed phosphorous groups on cell membrane.[28] However, it will prevent the particles from assembling on cells due to the strong electrostatic repulsion. As shown in Figure S4, Supporting Information, the bacterial cells were in poor contact with I-HTCC before modification, which was not favorable for the photoelectron delivery. Therefore, the positively charged poly (allylamine hydrochloride) (PAH) was used to modify the cell surface.[29] Before assembling the PBSs, the influence of PAH on bacterial viability was monitored (Figure S5, Supporting Information). There was no decrease in cell density with the modification of PAH after 24 h, indicating that the surface modification of bacterial membrane had no apparent influence on cell growth. Consistently, the *E. coli* cells maintained the healthy state with smooth and intact membrane after PAH modification (Figure 1b). Similar to this result, the production of shikimic acid by yeast (*Saccharomyces cerevisiae*) was unaffected with the modification of PAH.[14] This might be caused by the excellent adaptability of heterotrophs via the exportation of protons that coupled to oxidative reactions in the membrane.[30] After treating with PAH, the surface charge of the cell membrane converted to +51.60 mV (Figure S3b, Supporting Information), enabling the self-assembly process of the biohybrid system. After integration, the zeta potential ($\zeta$) of the biohybrid system was +9.57 mV, indicating the successful adhesion of the I-HTCC and *E. coli* cells driven by the electrostatic attractions.

On the other hand, the average size of biohybrid system was increased compared with that of the pure *E. coli* cultures (Figure S6, Supporting Information), an evidence that also indicated the self-assembly of I-HTCC and *E. coli* cells. Coincided with this result, the transmission electron microscopic (TEM)

images directly showed that the I-HTCC were closely attached to the surface of bacterial cells after modification (Figure 1d,e). Interestingly, the I-HTCC@*E. coli* system was tightly integrated even after centrifugation, whereas the simple mixture of I-HTCC and *E. coli* without surface modification (I-HTCC+*E. coli*) was separated (Figure S7, Supporting Information). This suggested that the self-assembled biohybrid system was stable even under strong centrifugal force. The photoelectrons transfer in the biotic–abiotic interface is the rate-determining step for the light-driven $H_2$ production of PBSs.[31] And the electrons can be directly delivered to bacteria through the redox proteins in the outer membrane or the soluble redox shuttles.[32] Therefore, with this delicate self-assembled biohybrid system, the photo-generated electrons were expected to transfer from I-HTCC to bacterial cell membrane without sluggish kinetics compared to that of in the suspended systems, which mediated by electron transfer agents such as MV.[6b] Besides, the well coated I-HTCC might also act as solid-state electron mediators for electron relay within the membrane owing to the good conductivity of I-HTCC.[31] However, the perturbation of injected electrons on the microbial metabolism and S2C conversion is still poorly understood and needed further investigation.

### 2.2. $H_2$ Production Performance and the Role of Photoelectrons

To demonstrate the applicability of the I-HTCC@*E. coli* biohybrid system, $H_2$ production under different VL intensities ($\lambda > 420$ nm) were conducted. No detectable $H_2$ evolution was observed with the pure I-HTCC under identical conditions (data not shown in the figure). As shown in **Figure 2**a, the level of $H_2$ production of the I-HTCC@*E. coli* biohybrid and the pure bacterial culture were almost the same in the dark (VL intensity = 0 W $m^{-2}$), whereas the $H_2$ production of the biohybrid was consistently higher than that of the pure bacterial culture under different intensities of VL. This suggested that the photoelectrons might be utilized by *E. coli* cells to power the $H_2$ production. With an increment of VL intensity, the $H_2$ production efficiency increased and reached 2.12 mM under 2000 W $m^{-2}$, a value that was 57.04% higher than that of the pure *E. coli* cultures. This was reasonable since more energetic electrons can be produced under stronger light intensities, as those demonstrated from photocurrent responses (Figure 1f). However, the $H_2$ production of the biohybrid system decreased with further increased light intensities (3000 and 4000 W $m^{-2}$), especially for the pure culture groups, most likely due to the photodamage caused by the strong light.[18] Although bacteria

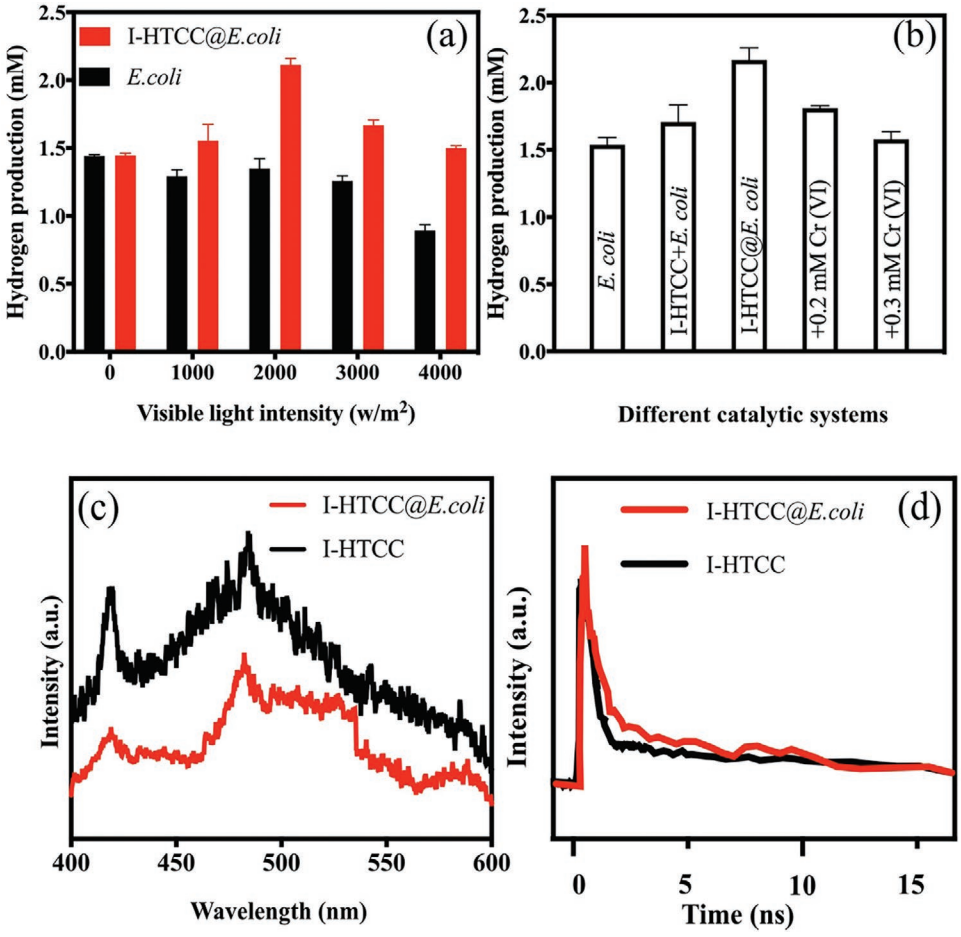


**Figure 2.** a) $H_2$ production of pure *E. coli* cultures and I-HTCC@*E. coli* biohybrid system with equal volume under irradiation of different VL intensities after 3 h. b) Separation and electron-scavenger studies under irradiation of 2000 W $m^{-2}$ for 3 h. c) Steady-state PL spectra of I-HTCC@*E. coli* and I-HTCC. d) TA spectra of I-HTCC@*E. coli* and I-HTCC.

could self-repair at a certain extent, this process was energy-consuming, which may take away the energy flow from $H_2$ production.[33] This led to the reduced production of $H_2$ in the biohybrid system. In addition, the calculated quantum efficiency (QE) of the biohybrid system was 9.11% under irradiation of 700-nm monochromatic light (Figure S8, Table S1, Supporting Information), which was an order-of-magnitude comparable to the year-long averages determined for plants and algae (0.2–1.6%).[34] And our system also showed comparable conversion efficiency compared with the existing PBSs (Table S2, Supporting Information).The high QE in the NIR region was due to the broad light absorption ability of I-HTCC, an observation that was well corresponded with the UV–vis–DRS result (inset of Figure 1c).

In order to investigate the electron transduction in the biohybrid system, a series of electron transfer studies were conducted under VL (2000 W $m^{-2}$). As those shown in Figure 2b, the $H_2$ production was only slightly increased with the simple mixing of I-HTCC and untreated *E. coli* cells, which was caused by the random electrons diffusion across cell membrane.[31] Therefore, increasing in $H_2$ production of I-HTCC@*E. coli* biohybrid system indicated that the close interfacial interactions between I-HTCC and *E. coli* was essential for the electrons delivery. To confirm the role of photoelectrons in $H_2$ production, the scavenger study was performed with the supplement of Cr (VI), a strong oxidant, in the biohybrid system. The working concentrations of Cr (VI) were optimized in preliminary studies owing to its cellular toxicity (Figure S9, Supporting Information). The $H_2$ production from biohybrid system diminished significantly upon the addition of 0.2 mM Cr (VI), and the addition of 0.3 mM Cr (VI) lowered the $H_2$ production to the level that native *E. coli* did. This was caused by the blocking of the extracellular electron transfer, in which Cr (VI) could rapidly diffuse to the biotic–abiotic interface due to its small size (0.44 Å) under stirring.[35] The separation and transfer of photogenerated charge carriers of hybrid system and pure I-HTCC suspensions had been investigated with the steady-state photoluminescence (PL) (Figure 2c). The PL emission intensity of the hybrid system was lower than that of the pure I-HTCC, which implied the successful delivery of the photoelectrons to bacterial cells and therefore increased the recombination time of charge-carriers. The photoelectrons transfer rates of pure catalyst and hybrid system were monitored by the transient absorption (TA) spectra (Figure 2d). The photoelectrons of hybrid system decayed slower than that of the I-HTCC, indicating that the photoelectrons from I-HTCC were efficiently transferred to the cells in hybrid system and thus suppressed its recombination rate. Fitting the TA data with exponential decay revealed that the hybrid system had a longer lifetime (160.12 ns) than that of the I-HTCC (68.14 ns), indicating that the photoelectrons were effectively separated and transferred to cells. This finding was consistent with the previous reported $Cu_2O$/RGO/*Shewanella oneidensis* system.[31] Overall, these results suggested that the electron transfer pathway at the interface of I-HTCC and *E. coli* cells was established and played an important role for the photo-enhanced $H_2$ production in the biohybrid system.

### 2.3. Photoelectrons Transduction Ways

After the role of photoelectrons had been confirmed, the transduction ways of photoelectrons to cells were then investigated. It was reported that the photoelectrons could energize the biological $H_2$ production through the direct electron transfer via membrane-bounded proteins (hydrogenase and cytochrome c) and indirect nicotinamide adenine dinucleotide (NAD)H-mediated process.[15] As the CB of I-HTCC was –0.53 V versus NHE (Figure S2, Supporting Information), theoretically the transfer of photoelectrons to membrane-bounded proteins (MBPs, ≈–0.3–0 V vs NHE) and NADH/$NAD^+$ ($E$ = –0.32 V vs NHE) was thermodynamically favored.[31] To prove the direct electron transfer from I-HTCC to cells, different concentrations of ionophores (2,4-DNP) were applied. Ionophores can disrupt electron transfer chain and inhibit the generation of ATP in cells, thus blocking $H_2$ yield with the consumption of sugar.[36] The concentration of 2,4-DNP were preoptimized to maximize the block effect but avoided toxicity to cells (Figure S10, Supporting Information). As shown in **Figure 3**a, the decrease of $H_2$ production that resulted from the increment concentration of ionophores revealed a pathway of direct electron transfer to the biological $H_2$ production pathway. Interestingly, the $H_2$ production at the presence of 0.5 mM ionophores (1.41 mM) was slightly higher than that of the pure cultures (1.35 mM). This not only confirmed the stable electron transfer on the biotic–abiotic interface of the present PBSs. It also

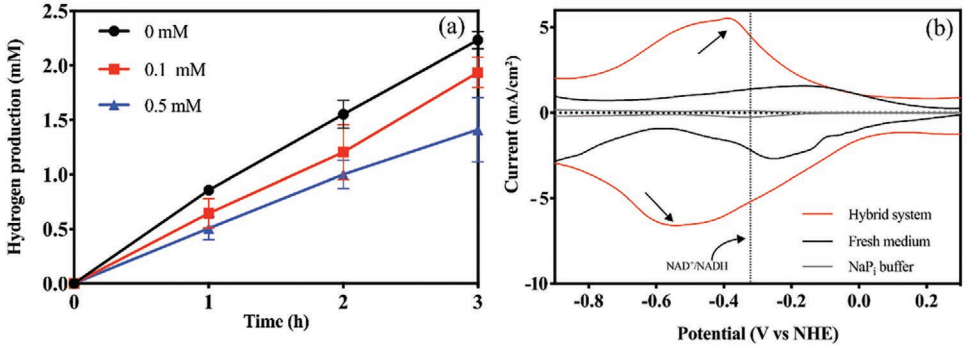


**Figure 3.** a) $H_2$ production of I-HTCC@*E. coli* biohybrid system with different concentration of (2,4-DNP) under irradiation of 2000 W $m^{-2}$. b) Differential pulse voltammetry of I-HTCC@*E. coli* biohybrid system and fresh medium with pure *E. coli* cultures. Arrows indicate possible electrochemical reduction of $NAD^+$ to NADH. $NaP_i$, sodium phosphate (referred to control).

implied that additional indirect electron transduction pathway may also be presented in the system, which mediated by the $NADH/NAD^+$.

The $NAD^+$ could serve as the photoelectrons acceptors and transform to NADH, which provides key reducing power in the energy-conserving redox reactions such as anaerobic fermentation.[37] This process is a common bottleneck for chemical conversion and was reported to linearly correlate with $H_2$ yield in microorganisms.[38] Therefore, the electron transfer to $NAD^+$ before and after reaction was investigated through the differential pulse voltammetry (Figure 3b).[14] It was observed that the biohybrid system exhibited more negative peaks than that of the thermodynamic potential for $NADH/NAD^+$, whereas the fresh medium showed small positive peaks. This phenomenon indicated that the possible electron transfer from I-HTCC to $NAD^+$ during the reaction. This might be induced by the soluble redox-active species excreted by *E. coli* cells, as these molecules were reported to involve in the electron transfer even without exogenous mediators.[39] Furthermore, in vitro reduction experiment with direct exogenous addition of $NAD^+$ was performed to prove the direct relationship between photoelectrons and the reducing power (Figure S11, Supporting Information). The concentration of NADH was increased with the prolonged reaction time in the light irradiation group, whereas it almost remained unchanged at very low concentrations in the dark. This indicated that the photoelectrons from I-HTCC could directly reduce $NAD^+$ to NADH, further confirming the indirect electrons mediated transfer ways. Even though, the electron transduction ways would differ from each other with different photosensitizers and bacterial species in various PBSs, which remains an active subject to be investigated. As for present system, the photoinduced electrons had been proved to transfer through two different pathways: the direct electron injection and the indirect NADH/ $NAD^+$ mediation.

### 2.4. Influence of the Photoelectrons on Cellular Metabolism

Due to the constant $H_2$ production among I-HTCC@*E.coli* in the dark and bare *E. coli* cells under dark or light, the metabolites of these groups were compared to confirm the importance of the metabolic pathway on the $H_2$ production. It was found that the change of metabolites for the *bare E. coli* cells under dark and light were almost the same as that of the biohybrid system in the dark (Figure S12, Supporting Information). The consistent trend could be ascribed to the same growth condition for these groups as there was no production of photoelectrons as well as the growth inhibition caused by the light or the catalyst. And these results suggested the important role of photoelectrons on the regulation of $H_2$ production through the metabolic pathways. After that, a series of experiments based on the $H_2$ production pathways were conducted for the biohybrid system in dark and light. The formate pathway and NADH pathway are two of the main $H_2$-producing ways in *E. coli* cells during anaerobic fermentation, both of which were originated from the glycolysis process.[40] The glucose is the original energy source and can be metabolized to a series of down-stream key intermediates for $H_2$ production.[41] Therefore, the glucose utilization efficiency was first monitored (**Figure 4**b) concurrently with the $H_2$ production under different time intervals (Figure 4a). It was rapidly utilized in the first 60 min for the light groups compared with that of the dark groups. The accelerated glycolysis was achieved through the rapid regeneration of NADH with the supplement of photoelectrons under irradiation. It has been reported that the NADH could positively regulate the glycolysis by acting as a co-factors for the glycolytic key enzyme, glyceraldehyder-3-phosphate dehydrogenase.[37] Consistent with the elevated glycolysis was the production pyruvate, the end-product of glycolysis, which increased and was higher for the light-irradiated groups than that of the dark groups in the first 60 min (Figure 4c). Pyruvate is the central intermediate in the heterotrophic carbon metabolism flux. It can be converted via lactate dehydrogenase (LDH), pyruvate formate lyase (PFL), and the pyruvate dehydrogenase complex (PDHc) to give the product of lactate, formate, and acetyl-CoA, respectively.[42] Therefore, the subsequent transformation of pyruvate caused a minor decrease trend in the late 30 min, which processed quickly for the light-irradiated groups with the mediation of photoelectrons. The lower accumulation of the lactate was observed in the light-irradiated groups (Figure 4d), suggesting that the photoelectrons probably inhibited the unfavorable metabolic pathways and caused the accumulation of pyruvate. Besides, the conversion by either PFL or the PDHc can be considered as a major switch point between fermentative routes (mixed acid fermentation) and oxidative respiratory pathway.[43] The PFL activity was higher in the light than that of in the dark across the reaction time, whereas the PDHc activity was still lower in the light than that of in the dark (Figure 4e,f). It has been reported that the PDHc activity under anaerobic conditions in *E. coli* was significantly inhibited by the NADH.[44] Thus, the higher reduced environment mediated by the injected photoelectrons led to the suppression of PDHc activity. The regulation of in vivo PFL activity is very complex, which associates with a series of factors like the oxygen status and reducing equivalents.[43] The increased activity of PFL was probably ascribed to the increment of NADH in the anaerobic conditions. As the PFL was encoded by the focApfl operon, the expression of *focApfl* was monitored directly as a chromosomal lacZ fusion.[45] The expression of *focApfl* operon was significantly increased for the biohybrid in the light compared with that of in the dark or the bare *E. coli* cells (Figure S13, Supporting Information), which was well coincided with the increased PFL activities for the biohybrid. As mentioned above, the transformation of pyruvate by the PDHc is a branch point for the oxidative respiratory pathway. At the second branch point, the acetyl-CoA can be converted to the fermentation products of acetate and ethanol or can subsequently undergo further oxidation in the tricarboxylic acid (TCA) cycle. The low activity of PDHc inhibited the production of acetyl-CoA (Figure 4g). And the lower concentration of acetyl-CoA and the anaerobic condition collectively inhibited the TCA cycle. Therefore, more energy was flowed toward the formation of formic acid, the precursor for $H_2$ production. In line with these results, a higher concentration of formate was accumulated in the first 60 min but then rapidly utilized in the late 30 min for the irradiated groups (Figure 4h). However, it increased slowly during the first 30 min, followed by a slow and steady decrease during the remaining reaction period for the dark groups. This implied

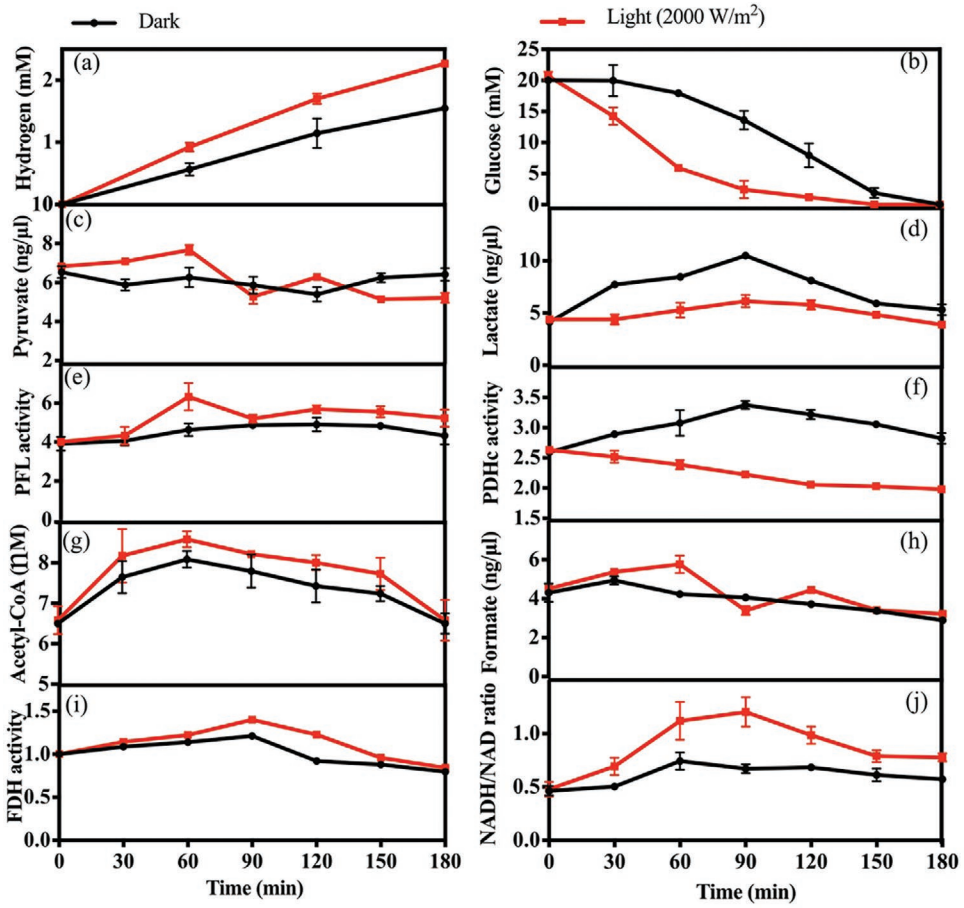


**Figure 4.** Mechanistic studies. a) $H_2$ production, b) glucose utilization, c) pyruvate concentration, d) lactate concentration, e) pyruvate formate lyase (PFL) activity, f) pyruvate dehydrogenase complex (PDHc) activity, g) acetyl-CoA concentration, h) formate concentration, i) formate dehydrogenase activity (FDH), and j) NADH/$NAD^+$ ratio of the biohybrid system in the dark or under irradiation of VL.

that the injected electrons could promote both the transformation of pyruvate to favorable formate and accelerate its utilization at the same time. A minor increase of formate production from 90 to 120 min was observed for the irradiated groups, which was similar to the trend of pyruvate production. This is the indication of direct energy flow from pyruvate to formate mediated by the electrons. The increased formate production thus resulted in the enhanced $H_2$ production in the biohybrid system, which was consistent with the above-mentioned $H_2$ production results. In addition, the formate dehydrogenase (FDH) was also measured (Figure 4i), which catalyzes the decomposition of formate to $H_2$ during anaerobic growth.[46] The higher catalytic activity of FDH pushed more energy into $H_2$ formation, resulting in higher $H_2$ accumulation for light-irradiated groups. This was potentially caused by the substrate promotion and simultaneously photoelectrons stimulation effect, as the standard thermodynamic driving force for the $H_2$ evolution reaction is small.[47]

The NADH pathway is complex and its metabolic mechanism is unclear. It not only serves as electrons acceptors in the breakdown of above-mentioned intermediates, but also directly release of $H_2$ with the ferredoxin (Fd)-$NAD^+$ reductase to balance the reducing power pool in the *E. coli* cells.[48] This process can be promoted by the exogenous electrons. Since the lactate formation is the most NADH-consuming pathway in glycolysis, its production thus became one of the key factors that influences the $H_2$ production.[40] The decreased concentration of lactate for light groups corresponded to the accumulate of intracellular NADH, and the photoelectron-powered NADH regeneration was thermodynamically favored and existed as above-mentioned. Therefore, the NADH/$NAD^+$ could be rapidly recycled driven by the injected photoelectrons. These factors altogether resulted in higher ratios of NADH/$NAD^+$ for the light-irradiated groups than that of dark groups during the entire reaction period (Figure 4j). On the other hand, it was reported that the NADH could be catalytically regenerated from the $NAD^+$-dependent FDH.[49] Therefore, the increased FDH activity along with the injected photoelectrons also facilitated the increase of NADH/$NAD^+$ in the first 90 min of reaction. Although the minor increase ratio of NADH/$NAD^+$ could regulate the biological $H_2$ pathway, the excess electrons and reducing equivalent would damage bacterial cells.[50] The intracellular redox regulation effects responded to such elevated reductive stress via up-regulated the NADH to $H_2$ conversion, which led to the decline of NADH/$NAD^+$ ratio and additional $H_2$ production for the light groups during the reaction period

that longer than 90 min. It is worth noting that, owing to the complexity of cellular metabolism, the NADH pathway was inextricably tied up with formate pathway, which could not be reflected in a quantitative manner except for the production of $H_2$. In summary, both the NADH pathway and formate pathways promoted by the photoelectrons, together contributed to the enhanced $H_2$ production in the biohybrid system under light irradiation.

### 2.5. Proposed Mechanism

Combining the results of the photo electrons transduction and its role in biological $H_2$ production, the mechanism of photo-enhanced $H_2$ production in the I-HTCC@*E. coli* biohybrid system was proposed and schematically illustrated in **Scheme 1**. After the surface modification of the bacterial cell membrane by PAH, the I-HTCC@*E. coli* biohybrid system was self-assembled through the electrostatic interactions. With the irradiation of VL, the photoelectrons from the I-HTCC were directly delivered to bacterial cells via the MBPs, or indirectly mediated by NADH/$NAD^+$. The photoelectrons then fine-tuned the biological $H_2$ production pathway in a subtle manner. Initially, it promoted the intracellular glycolysis and therefore accelerated the glucose utilization and pyruvate accumulation. In the meantime, the lactate fermentation and acetyl-CoA production were inhibited by the excess photoelectrons, which directed more energy flux to the formation of formic acid. This thus lowered the formation of byproduct (lactate and acetyl-CoA) and, in turn, facilitated the increase of pyruvate and NADH, which then led to the further enrichment of formate for $H_2$ production via the formate pathway. The FDH catalytic activity was strengthened by the additional photoelectrons and increased formate substrate effect, which was beneficial for the rapid decomposition of formate coupled with the higher $H_2$ production efficiency. As for the NADH pathway, the elevated intracellular NADH/$NAD^+$ ratio not only up regulated the biological $H_2$ production pathway but also led to the release of $H_2$, both effects that eventually resulted in the generation of additional $H_2$. It is therefore reasonable to conclude that the enhanced the $H_2$ production in the biohybrid system under VL irradiation was mainly due to the following effects: the promotion of metabolic pathways that favor the $H_2$ production (e.g., increased production of formate and NADH), and the inhibition of metabolic pathways that

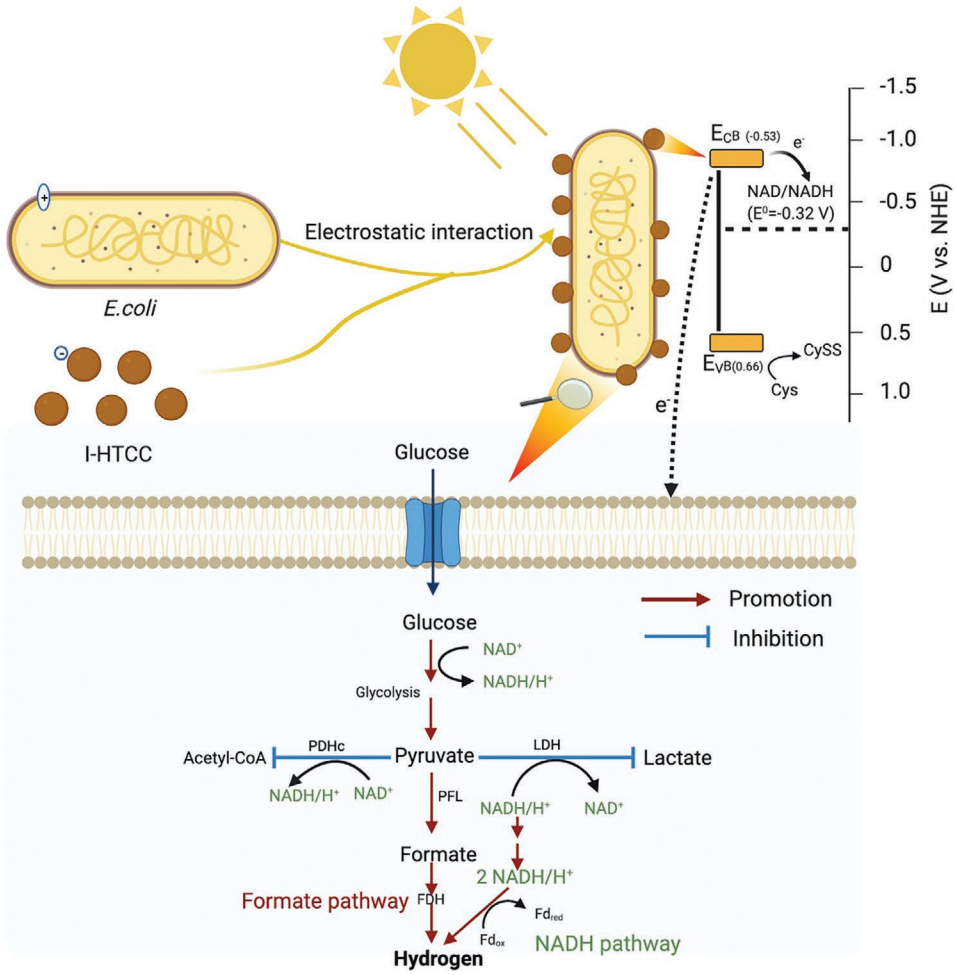


**Scheme 1.** Proposed schematic mechanism for the photo-enhanced $H_2$ production in the I-HTCC@*E. coli* biohybrid system. Abbreviations: conduction band (CB), valence band (VB), cysteine (Cys), cystine (Cyss), ferredoxin (Fd).

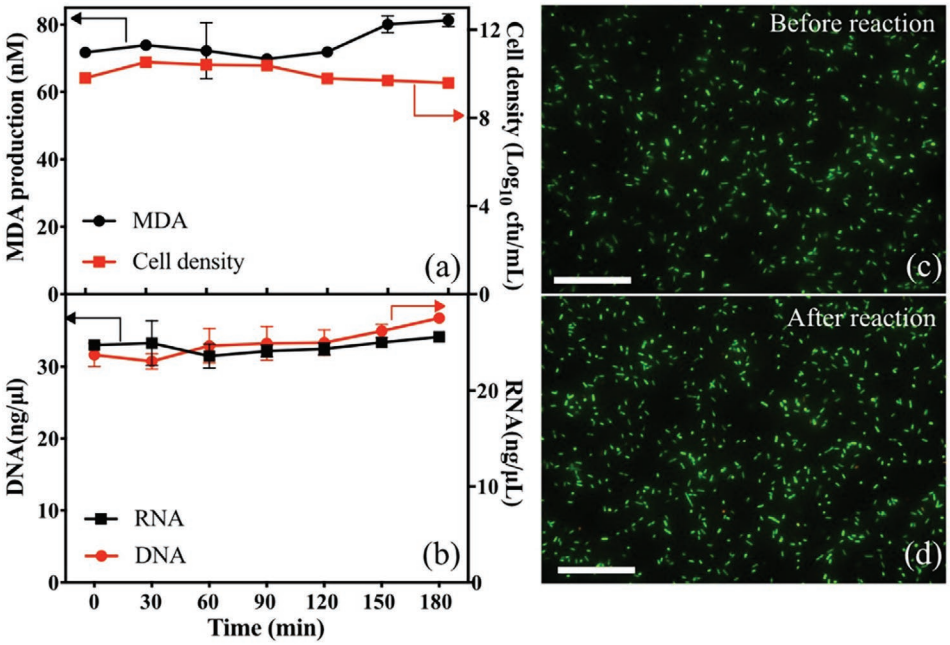


**Figure 5.** a) Cell viability and MDA production, b) leakage of the DNA and RNA during the $H_2$ production process in the biohybrid system, c,d) the fluorescence microscopic images of bacteria before and after $H_2$ production reaction (scale bar: 10 μm).

impair the $H_2$ production (e.g., reduced lactate formation and acetyl-CoA), as well as the enhanced catalytic power of the key enzymes (e.g., higher PFL and FDH activities).

### 2.6. Biocompatibility of the Hybrid System

Although the enhanced $H_2$ production from the I-HTCC@*E. coli* biohybrid system was promising, the biocompatibility of the system may affect its potential application. Therefore, the cell viability, membrane integrity, and the leakage of intracellular substances in I-HTCC@*E. coli* system were monitored during the $H_2$ production process. As presented in **Figure 5**a, the cell viability remained almost unchanged during the entire reaction period, indicating that both the light intensity and the I-HTCC NPs did not affect cell growth. The bacterial membrane consists of phospholipid bilayers,[51] thus the peroxidation intermediate MDA was measured to reflect the levels of membrane oxidation. The MDA concentration was stable state in the first 120 min, followed by a slight increase in the last 60 min. However, there was no significant difference ($p < 0.05$) between the MDA concentrations measured at 0 and 180 min. The minor increase of MDA might be caused by the metabolizing and dissolving of the organics with the prolonged reaction time. The leakage of DNA and RNA is lethal to the bacterial. No obvious leakage of DNA and RNA was observed during the reaction period (Figure 5b), indicating the integrity of the cell membrane. To further confirm this observation, the fluorescence stain was conducted (Figure 5c,d). The cells before and after the reaction were stained with the dye mixture. Cells with intact membrane emit green fluorescence, and those with damaged cell membranes emitted red signals.[51] The consistent green fluorescence signals gave rise by the *E. coli* cells before and after reactions suggested they were in a healthy state throughout the $H_2$ production process. All of the above-mentioned evidence illustrated that both the fabrication and reaction processes were biocompatible to bacterial cells, which ensured its potentials for practical applications.

### 2.7. Stability and Application of the Hybrid System

After verifying the biocompatibility of the present system, the feasibilities of the system for the potential applications were evaluated. First, the reaction stability of the biohybrid system was measured (**Figure 6**a). The $H_2$ production efficiency remained stable during the first three cycles. However, the accumulation of secondary metabolites with the extended reaction time probably influenced metabolic activities and competed for photoelectrons with bacterial cells.[52] Therefore, a small and insignificant ($p < 0.05$) reduction of $H_2$ production was observed from the last two cycles. This problem can be mitigated via in situ refreshment of the reaction medium.[53] The biohybrid after the reaction was also observed under the TEM. As displayed in Figure 6d, the bacterial cells after reaction still featured integral membrane structure, and their overall morphologies were highly similar to those before the reaction. Moreover, the I-HTCC particles still attached to the bacterial membrane without falling off, indicating the relative stability of the self-assembly structure. The $H_2$ production of the biohybrid system under simulated sunlight and full spectrum (2000 W $m^{-2}$) were evaluated the potentials of the biohybrid system for practical applications (Figure 6b). Due to the harmful effect of the ultraviolet in simulated sunlight and full spectra (Figure S14, Supporting Information), the $H_2$ production decreased for both the pure *E. coli* cultures and the biohybrid system with these

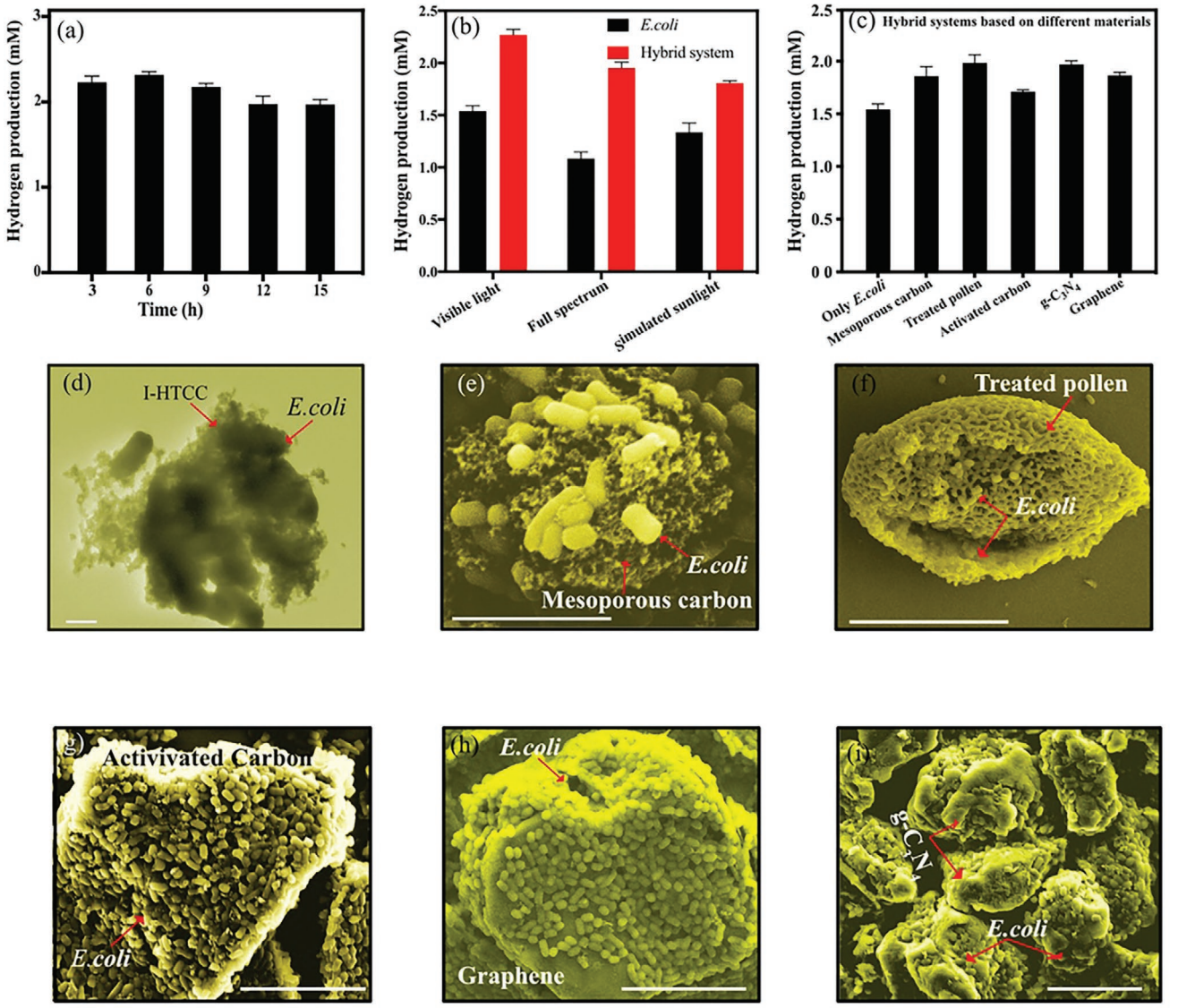


**Figure 6.** $H_2$ production of the I-HTCC@*E. coli* biohybrid system a) after five cycles, b) $H_2$ production of the I-HTCC@*E. coli* biohybrid system with irradiation of different light sources (2000 W $m^{-2}$), b) $H_2$ production with different carbon-based materials and *E. coli* biohybrid systems under irradiation of VL (2000 W $m^{-2}$), d) SEM image of the I-HTCC @ *E. coli* biohybrid system after reaction (scale bar: 1 µm). TEM image of *E. coli* cells assembled with e) mesoporous carbon, f) acid-treated pollen, g) activated carbon, h) graphene flakes, and i) g-$C_3N_4$ (scale bar: 10 µm).

light sources. Still, the biohybrid system also outweighed to the pure cultures, as suggested by the significant difference in $H_2$ production ($p < 0.05$).

To better evaluate the practical application of the I-HTCC@*E.coli* biohybrid system, different water samples collected from Lam Tsuen river and Tai Po Sewage Treatment Works together with the tap water sample were applied for $H_2$ production under simulated sunlight (Figure S15, Supporting Information, AM1.5 filter, 2000 W $m^{-2}$). Key physiochemical parameters of the water samples were determined and listed in Table S3, Supporting Information. There was a slight decrement in $H_2$ production for the tap water without significant difference ($p < 0.05$), which might be caused by the influence of cell homeostasis in water sample than that of in medium.[54] However, the further decrement of efficiency for the Lam Tsuen river was probably caused by the quench effect of anions to the photoelectrons and poor nutrition condition, whereas the increased efficiency in the effluent compared with that of in river might be attributed to the dissolved organic matters, which could supply additional nutrient to bacteria while simultaneous competition with photoelectrons.[3b] Due to the relative complex components in the natural water samples, more efforts might be also devoted to optimizing the efficiency of the I-HTCC@*E.coli* biohybrid system with the cultures and solar sources. Importantly, the feasibility of $H_2$ production in the natural water samples with simulated sunlight highlighted that the possibility of using sunlight as an energy source to trigger the I-HTCC@*E. coli* biohybrid system in natural water samples for S2C conversion.

To test the feasibility of the simple "add-on" mode, negatively charged carbon-based materials were assembled with positively

charged *E. coli* cells, including mesoporous carbon, acid-treated pollen, activated carbon, g-$C_3N_4$, and graphene flakes (Figure 6c; Table S4, Supporting Information). An increase of 11–28.57% on $H_2$ production were observed from different carbon-based materials@*E.coli* biohybrids, as compared with that of the pure *E. coli* cultures, whereas no detectable $H_2$ can be confirmed from the pure catalysts under the same condition. The promotion effect might be further enhanced with material chemistry, such as shape engineering of g-$C_3N_4$ with sharp edges[55] and synthesis of composite catalyst with carbon-based templates.[56] As shown in Figure 6e–i, the bacterial cells were closely and extensively attached to these carbon-based materials. Such mode of material-cell interaction improved the electron transfer thus enhancing the $H_2$ production efficiency of the hybrid system. However, due to the different size of materials and bacterial species, the ratio of bacteria and material needed to be further optimized when applied to different PBSs. These results suggested that the versatility of the proposed "add-on" mode for biohybrid fabrication in scaling-up applications or assembling bacteria with other materials under easy operation.

## 3. Conclusions

In summary, the I-HTCC@*E. coli* biohybrid system has been successfully fabricated for enhanced $H_2$ production via the facile "add-on" mode. The mechanistic study deepened the understanding of the transduction ways of photoelectrons and their roles on the regulation of biological $H_2$ pathways. The stability and biocompatibility of the biohybrid system implied the potential practical application of the proposed "add-on" mode. The broad applicability on a series of negatively charged carbon-based materials indicated the wide adaptability of the "add-on" mode, which provided new insights into the rational design of the whole-cell PBSs for enhanced $H_2$ production performance. Benefited from the mature genetic manipulation on the metabolic pathways of *E. coli*, the product diversity and catalytic conversion efficiency can be further optimized in the future study. The charge and energy transfer at the biotic–abiotic interface can be further explored in the present system with the synthetic biology tools, which is essential for maximizing efficiency and longevity of the PBSs. Therefore, the present hybrid system shows both theoretical and practical significances and can be further upgraded with the development of material chemistry and synthetic biology.

## 4. Experimental Section

*Modular Assembly of the I-HTCC@E. coli Biohybrids*: The I-HTCC nanoparticles (NPs) were synthesized through a one-pot hydrothermal approach. Typically, 0.5 g of elemental iodine was dissolved in 60 mL of absolute ethanol, then mixed with 5 mL glucose solution (0.4 g $mL^{-1}$). The mixture was sonicated for 30 min, then transferred to a 100 mL of Teflon-lined stainless-steel autoclave and maintained at 200 °C for 24 h. The I-HTCC product was filtered and washed with deionized water, then dried in a vacuum oven overnight. The I-HTCC was carefully grinded and dispersed in deionized water for sonication. After that, the I-HTCC was centrifuged at 8000 × *g* for 5 min to collect the nano-sized I-HTCC samples.

The *E. coli*-K12 (MG1655) was inoculated in LB medium and incubated at 37 °C for 16 h. Then the bacterial culture was collected via centrifugation at 10 000 × *g* for 10 min and washed with sterilized water. The cells were re-suspended in BC medium (Table S1, Supporting Information) supplied with 30 mM glucose, and then anaerobically cultured at 37 °C for 12 h.[57] After that, poly (allylamine hydrochloride) (PAH, 5 mg $mL^{-1}$) was added to the cell suspension and gently shook in a 2.5 L of anaerobic jar (Oxoid AG0025A, UK) for 20 min. The cells were washed with sterilized water to remove excess PAH molecules. The addition concentration of I-HTCC was spectrophotometrically recorded and optimized (Figure S16, Supporting Information) using a UV–vis spectrometer (BlueStar A Split Beam, LabTech, USA). Finally, the cells suspension was mixed with I-HTCC (adjusted to 0.5 g $L^{-1}$) and anaerobically stirred for 30 min to facilitate the assembly process.

*Characterization of the I-HTCC@E. coli Biohybrids*: The XRD pattern was analyzed by a SmartLab X-ray diffractometer (Rigaku Corporation, Japan) with Cu K$\alpha$ radiation. The morphology of I-HTCC was observed by TEM using a Tecnai F20 TEM (FEI, Hillsboro, OR) equipped with EDX spectroscopy. The UV–vis DRS spectrum of I-HTCC was measured with a PerkinElmer Lmabda 950 spectrometer. The photoluminescence and transient absorption spectroscopy studies were conducted with FP-6500 fluorescence spectrometer (Jasco, Japan) and Femtosecond Transient Absorption Spectrometer (Helios, ultrafast systems). Before the measurement, the hybrid system was washed with sterilized deionized water for several times to exclude the secretions after integration and monitored in water. The photocurrent and Mott–Schottky measurements of I-HTCC were studied by an electrochemical workstation (CHI650E, CH Instruments, USA). The size distribution and zeta potential ($\zeta$) of the samples were measured with a Zetasizer Nano (ZS90, Malvern, UK).

*$H_2$ Production and Quantum Efficiency Measurement*: The I-HTCC@*E. coli* biohybrid was resuspended in simplified BC medium (Table S1, Supporting Information) with 20 mM glucose and 1 mM cysteine. Then the suspension was transferred to a cylindrical reactor (internal diameter = 76 mm, Beijing Perfectlight) and bubbled $N_2$ for 30 min. A xenon lamp (PLS-SXE300D, Beijing Perfectlight) equipped with 420 nm cut-off filter (light spectrum in Figure S17, Supporting Information) was used as the light source. The intensities of xenon lamp were adjusted to 0, 1000, 2000, 3000, and 4000 W $m^{-2}$ with a light meter (Model-250, LI-COR, USA), respectively. The reaction temperature was maintained at 37 °C using a circulating water bath (CW-05G, Jeiotech, Korea). During the reaction, the concentration of produced $H_2$ was determined at given time interval with a gas chromatography (GC-7806 with nitrogen as a carrier gas and 5 Å molecular sieve column, Shiweipx, China). As control groups, parallel anaerobic *E. coli* cultures without I-HTCC were performed at the same conditions.

The QE was measured under the condition that identical to those applied for $H_2$ production except under different monochromatic light (470, 525, 570, 620, and 700 nm). The QE was calculated with the following equation:

$$QE = \frac{N_{H_2}}{N_p} = \frac{2 \times \text{the number of additional evolved } H_2 \text{ molecules}}{\text{the number of incident photones}} \times 100\% = \frac{2 \times N_a \times M_{H_2}}{\frac{PSt\lambda}{hc}} \times 100\% \quad (1)$$

where $N_a$, $M_{H2}$, $P$, $S$, $t$, $\lambda$, $h$, and $c$ are the Avogadro's constant, moles of $H_2$ (mol), power of the Xenon lamp at a certain wavelength (W $m^{-2}$), active area ($cm^2$), reaction time (h), incident light wavelength (nm), Planck constant (J•s), and speed of light (m $s^{-1}$), respectively.

*Electron Transduction and Bacterial Metabolism Study*: To confirm the role of the close attachment of I-HTCC with *E. coli* cells for electrons delivery, the untreated *E. coli* cells were simply mixed with the same amount of I-HTCC, which was denoted with I-HTCC+*E. coli*. The scavenger study was conducted with the addition of 0.2 and 0.3 mM of Cr(VI) in the biohybrid system to quench the photogenerated electrons. The electrons transduction pathway study was conducted by adding 0.1 and 0.5 mM of 2,4-dinitrophenol (DNP) to suppress the NADH mediated electron transferring way. For all of the electron transfer

studies, the same $H_2$ production condition (SBC medium, 1 mM cysteine, 20 mM glucose, and 2000 W $m^{-2}$ of VL intensity) were applied.

The glucose utilization efficiency of the hybrid system was investigated by the dinitrosalicylic acid (DNS) colorimetric method.[58] The intracellular compounds were detected through the pyruvate assay kit (MAK071, Sigma-Aldrich), lactate assay kit (MAK065, Sigma-Aldrich), formate assay kit (MAK059, Sigma-Aldrich), acetyl-CoA quantification kit (MAK039, Sigma-Aldrich), and NADH/NAD ratio assay kit (MAK037, Sigma-Aldrich), respectively. The overall activity of the PDHc was measured spectrophotometrically by monitoring the reduction of ferricyanide at 430 nm ($\varepsilon$ = 1030 $M^{-1}$ $cm^{-1}$).[44] The PFL was monitored spectrophotometrically at 340 nm ($\varepsilon$ = 6.22 $mM^{-1}$ $cm^{-1}$).[59] The FDH activity was measured with the formate-dependent benzyl viologen (BV, Sigma-Aldrich) and expressed as the percent of BV reduced to the control group before reaction.[46]

*Biocompatibility and Stability Study*: At fixed time intervals, aliquots of reaction mixtures were collected by a sealing syringe. The solutions were serially diluted and spread on the nutrient agar plates (Lab M, Lancashire, UK). After incubation for 16 h at 37 °C, the colonies were recorded and calculated as CFU $mL^{-1}$. Parallelly, the collected samples were also used to analyze the oxidation degree of lipid with the Lipid peroxidation (MDA) Assay kit (MAK085, Sigma-Aldrich). The biohybrid samples before and after reaction were concentrated and stained with a fluorescent dye mixture prepared with the LIVE/DEAD BacLight Bacterial Viability Kit (L7012, Molecular Probes, Inc., Eugene, OR) and observed under a fluorescent microscope (ECLIPSE 80i, Nikon, Japan). The leakage of the DNA and RNA was monitored with Thermo Scientific NanoDrop spectrophotometers. The stability of the system was evaluated via performing five cycles of $H_2$ production under the same conditions. Typically, after each cycle reaction, the xenon lamp was turned off. The reaction solution was re-supplemented with 20 mM glucose and 1 mM cysteine and bubbled with $N_2$ until the signals of $H_2$ and $O_2$ were unable to be detected with GC.

The data were analyzed using Prism Grapad 8 and mean and statistical product and service solutions (SPSS) for Windows. Means were compared using least significant differences (LSD) calculated at a significance level of $p < 0.05$.

## Supporting Information

Supporting Information is available from the Wiley Online Library or from the author.

## Acknowledgements

B.W. thanks for the funding support from the National Key R&D Program of China (Grant No. 2020YFA0907400), National Natural Science Foundation of China (Grant No. 22008252), and CAS Key Laboratory of Quantitative Engineering Biology, Shenzhen Institute of Synthetic Biology, Shenzhen Institutes of Advanced Technology, Chinese Academy of Sciences. The research project was also supported by Technology and Business Development Fund, The Chinese University of Hong Kong (No. TBF18SCI006). Z.J. wants to thank the funding for Scientific Research Startup of Jiangsu University and Open Found of Guangdong Key Laboratory of Environmental Catalysis and Health Risk Control (GKECHRC-06).

## Conflict of Interest

The authors declare no conflict of interest.

## Data Availability Statement

Research data are not shared.

## Keywords

*Escherichia coli*, hydrogen production, iodine-doped hydrothermally carbonized carbon, mechanism, photosynthetic biohybrid systems

Received: January 26, 2021
Revised: March 20, 2021
Published online: April 21, 2021

[1] P. J. Williams, L. M. Laurens, *Energy Environ. Sci.* **2010**, *3*, 554.
[2] a) N. Kornienko, J. Z. Zhang, K. K. Sakimoto, P. Yang, E. Reisner, *Nat. Nanotechnol.* **2018**, *13*, 890; b) X. G. Zhu, S. P. Long, D. R. Ort, *Annu. Rev. Plant Biol.* **2010**, *61*, 235.
[3] a) R. E. Blankenship, D. M. Tiede, J. Barber, G. W. Brudvig, G. Fleming, M. Ghirardi, M. Gunner, W. Junge, D. M. Kramer, A. Melis, *Science* **2011**, *332*, 805; b) C. Zhao, Z. Chen, R. Shi, X. Yang, T. Zhang, *Adv. Mater.* **2020**, *32*, 1907296.
[4] J. L. Herek, W. Wohlleben, R. J. Cogdell, D. Zeidler, M. Motzkus, *Nature* **2002**, *417*, 533.
[5] A. S. Hawkins, P. M. McTernan, H. Lian, R. M. Kelly, M. W. Adams, *Curr. Opin. Biotechnol.* **2013**, *24*, 376.
[6] a) K. K. Sakimoto, A. B. Wong, P. Yang, *Science* **2016**, *351*, 74; b) Z. Chen, J. Zhou, Y. Wang, Y. Wang, *Curr. Opin. Biotechnol.* **2020**, *64*, 161.
[7] A. Krasnovsky, V. Nikandrov, *FEBS Lett.* **1987**, *219*, 93.
[8] a) B. Wang, C. Zeng, K. H. Chu, D. Wu, H. Y. Yip, L. Ye, P. K. Wong, *Adv. Energy Mater.* **2017**, *7*, 1700611; b) W. Wei, P. Sun, Z. Li, K. Song, W. Su, B. Wang, Y. Liu, J. Zhao, *Sci. Adv.* **2018**, *4*, eaap9253.
[9] J. Ye, J. Yu, Y. Zhang, M. Chen, X. Liu, S. Zhou, Z. He, *Appl. Catal. B* **2019**, *257*, 117916.
[10] B. Wang, Z. Jiang, C. Y. Jimmy, J. Wang, P. K. Wong, *Nanoscale* **2019**, *11*, 9296.
[11] M. Chen, X. F. Zhou, Y. Q. Yu, X. Liu, R. J. X. Zeng, S. G. Zhou, Z. He, *Environ. Int.* **2019**, *127*, 353.
[12] S. Huang, J. Tang, X. Liu, G. Dong, S. Zhou, *ACS Sustainable Chem. Eng.* **2019**, *7*, 15427.
[13] Z. Jiang, B. Wang, C. Y. Jimmy, J. Wang, T. An, H. Zhao, H. Li, S. Yuan, P. K. Wong, *Nano Energy* **2018**, *46*, 234.
[14] J. Guo, M. Suástegui, K. K. Sakimoto, V. M. Moody, G. Xiao, D. G. Nocera, N. S. Joshi, *Science* **2018**, *362*, 813.
[15] Y. Ding, J. R. Bertram, C. Eckert, R. R. Bommareddy, R. Patel, A. Conradie, S. Bryan, P. Nagpal, *J. Am. Chem. Soc.* **2019**, *141*, 10272.
[16] R. Shi, J. Guo, X. Zhang, G. I. Waterhouse, Z. Han, Y. Zhao, L. Shang, C. Zhou, L. Jiang, T. Zhang, *Nat. Commun.* **2020**, *11*, 1.
[17] S. Jin, Y. Jeon, M. S. Jeon, J. Shin, Y. Song, S. Kang, J. Bae, S. Cho, J. K. Lee, D. R. Kim, *Proc. Natl. Acad. Sci. U. S. A.* **2021**, *9*, 118.
[18] K. K. Sakimoto, N. Kornienko, P. Yang, *Acc. Chem. Res.* **2017**, *50*, 476.
[19] S. Galanie, K. Thodey, I. J. Trenchard, M. F. Interrante, C. D. Smolke, *Science* **2015**, *349*, 1095.
[20] A. Kumar, L. H.-H. Hsu, P. Kavanagh, F. Barrière, P. N. Lens, L. Lapinsonnière, U. Schröder, X. Jiang, D. Leech, *Nat. Rev. Chem.* **2017**, *1*, 0024.
[21] J. Nielsen, J. D. Keasling, *Cell* **2016**, *164*, 1185.
[22] Y. H. Ng, S. Ikeda, M. Matsumura, R. Amal, *Energy Environ. Sci.* **2012**, *5*, 9307.

[23] Z. Hu, Z. Shen, J. C. Yu, *Environ. Sci. Technol.* **2017**, *51*, 7076.
[24] a) K. Holá, M. V. Pavliuk, B. Németh, P. Huang, L. Zdražil, H. Land, G. Berggren, H. Tian, *ACS Catal.* **2020**, *10*, 9943; b) K. A. Brown, M. B. Wilker, M. Boehm, G. Dukovic, P. W. King, *J. Am. Chem. Soc.* **2012**, *134*, 5627; c) C. Tapia, S. Zacarias, I. A. Pereira, J. C. Conesa, M. Pita, A. L. De Lacey, *ACS Catal.* **2016**, *6*, 5691; d) E. Reisner, D. J. Powell, C. Cavazza, J. C. Fontecilla-Camps, F. A. Armstrong, *J. Am. Chem. Soc.* **2009**, *131*, 18457.
[25] A. W. Harris, J. N. Cha, *Mol. Syst. Des. Eng.* **2020**, *5*, 1088.
[26] P. W. King, *Biochim. Biophys. Acta, Biomembr.* **2013**, *1827*, 949.
[27] C. Aprile, A. Corma, H. Garcia, *Phys. Chem. Chem. Phys.* **2008**, *10*, 769.
[28] F. Jean-François, S. Castano, B. Desbat, B. Odaert, M. Roux, M.-H. Metz-Boutigue, E. J. Dufourc, *Biochemistry* **2008**, *47*, 6394.
[29] G. M. Chertow, S. K. Burke, J. M. Lazarus, K. H. Stenzel, D. Wombolt, D. Goldberg, J. V. Bonventre, E. Slatopolsky, *Am. J. Kidney Dis.* **1997**, *29*, 66.
[30] P. D. Damper, W. Epstein, *Antimicrob. Agents Chemother.* **1981**, *20*, 803.
[31] H. Shen, Y.-Z. Wang, G. Liu, L. Li, R. Xia, B. Luo, J. Wang, D. Suo, W. Shi, Y.-C. Yong, *ACS Catal.* **2020**, *10*, 13290.
[32] K. K. Sakimoto, N. Kornienko, S. Cestellos-Blanco, J. Lim, C. Liu, P. Yang, *J. Am. Chem. Soc.* **2018**, *140*, 1978.
[33] S. Cestellos-Blanco, H. Zhang, J. M. Kim, Y.-x. Shen, P. Yang, *Nat. Catal.* **2020**, *3*, 245.
[34] A. Larkum, *Curr. Opin. Biotechnol.* **2010**, *21*, 271.
[35] S. Lin, L. Xu, A. C. Wang, Z. L. Wang, *Nat. Commun.* **2020**, *11*, 1.
[36] R. J. Kessler, C. A. Tyson, D. E. Green, *Proc. Natl. Acad. Sci. U. S. A.* **1976**, *73*, 3141.
[37] W. Ying, *Front. Biosci.* **2006**, *11*, 3129.
[38] S. Li, Y. Li, C. D. Smolke, *Nat. Chem.* **2018**, *10*, 395.
[39] Y. Hubenova, M. Mitov, *Bioelectrochemistry* **2015**, *106*, 177.
[40] D. Liu, Y. Sun, Y. Li, Y. Lu, *Sci. Rep.* **2017**, *7*, 9587.
[41] P. C. Hallenbeck, J. R. Benemann, *Int. J. Hydrogen Energy* **2002**, *27*, 1185.
[42] J. T. Pronk, H. Y. de Steensma, J. P. van Dijken, *Yeast* **1996**, *12*, 1607.
[43] S. Alexeeva, B. de Kort, G. Sawers, K. J. Hellingwerf, M. J. de Mattos, *J. Bacteriol. Res.* **2000**, *182*, 4934.
[44] M. R. De Graef, S. Alexeeva, J. L. Snoep, M. J. T. de Mattos, *J. Bacteriol. Res.* **1999**, *181*, 2351.
[45] G. Sawers, B. Suppmann, *J. Bacteriol. Res.* **1992**, *174*, 3474.
[46] N. Mnatsakanyan, A. Vassilian, L. Navasardyan, K. Bagramyan, A. Trchounian, *Curr. Microbiol.* **2002**, *45*, 281.
[47] J. S. McDowall, B. J. Murphy, M. Haumann, T. Palmer, F. A. Armstrong, F. Sargent, *Proc. Natl. Acad. Sci. U. S. A.* **2014**, *111*, E3948.
[48] R. Porra, W. Thompson, P. Kriedemann, *Biochim. Biophys. Acta, Biomembr.* **1989**, *975*, 384.
[49] J. Wang, Y. Yang, R. Zhang, X. Shen, Z. Chen, J. Wang, Q. Yuan, Y. Yan, *Metab. Eng. Commun.* **2018**, *45*, 1.
[50] G. J. Schut, M. W. Adams, *J. Bacteriol. Res.* **2009**, *191*, 4451.
[51] K. Xiao, T. Wang, M. Sun, A. Hanif, Q. Gu, B. Tian, Z. Jiang, B. Wang, H. Sun, J. Shang, *Environ. Sci. Technol.* **2019**, *54*, 537.
[52] F. Pietra, *Nat. Prod. Rep.* **1997**, *14*, 453.
[53] S. Wallace, E. P. Balskus, *Angew. Chem., Int. Ed.* **2016**, *55*, 6023.
[54] Y. Sakiyama, T. Tomai, M. Miyano, D. Graves, *Appl. Phys. Lett.* **2009**, *94*, 161501.
[55] J. Zhang, M. Zhang, C. Yang, X. Wang, *Adv. Mater.* **2014**, *26*, 4121.
[56] Y. Zhu, L. Song, N. Song, M. Li, C. Wang, X. Lu, *ACS Sustainable Chem. Eng.* **2019**, *7*, 2899.
[57] A. Yoshida, T. Nishimura, H. Kawaguchi, M. Inui, H. Yukawa, *Appl. Environ. Microbiol.* **2005**, *71*, 6762.
[58] G. L. Miller, *Anal. Chem.* **1959**, *31*, 426.
[59] T. Rydzak, D. B. Levin, N. Cicek, R. Sparling, *J. Biotechnol.* **2009**, *140*, 169.